PAPER

Recombination radius of a Frenkel pair and capture radius of a self-interstitial atom by vacancy clusters in bcc Fe

IOP Publishing Journal of Physics: Condensed Matter
J. Phys.: Condens. Matter **27** (2015) 335401 (7pp) doi:10.1088/0953-8984/27/33/335401

Recombination radius of a Frenkel pair and capture radius of a self-interstitial atom by vacancy clusters in bcc Fe

Kenichi Nakashima[1,2], **Roger E Stoller**[1] **and Haixuan Xu**[3]

[1] Materials Science and Technology Division, Oak Ridge National Laboratory, Oak Ridge, TN 37831-6114, USA
[2] Materials Science Research Laboratory, Central Research Institute of Electric Power Industry, Komae-shi, Tokyo 201-8511, Japan
[3] Department of Materials Science and Engineering, University of Tennessee, Knoxville, TN 37996-2100, USA

E-mail: ken-ichi@criepi.denken.or.jp

Received 1 April 2015, revised 7 July 2015
Accepted for publication 9 July 2015
Published 4 August 2015

Abstract

The recombination radius of a Frenkel pair is a fundamental parameter for the object kinetic Monte Carlo (OKMC) and mean field rate theory (RT) methods that are used to investigate irradiation damage accumulation in irradiated materials. The recombination radius in bcc Fe has been studied both experimentally and numerically, however there is no general consensus about its value. The detailed atomistic processes of recombination also remain uncertain. Values from $1.0a_0$ to $3.3a_0$ have been employed as a recombination radius in previous studies using OKMC and RT. The recombination process of a Frenkel pair is investigated at the atomic level using the self-evolved atomistic kinetic Monte Carlo (SEAKMC) method in this paper. SEAKMC calculations reveal that a self-interstitial atom recombines with a vacancy in a spontaneous reaction from several nearby sites following characteristic pathways. The recombination radius of a Frenkel pair is estimated to be $2.26a_0$ by taking the average of the recombination distances from 80 simulation cases. In addition, we apply these procedures to the capture radius of a self-interstitial atom by a vacancy cluster. The capture radius is found to gradually increase with the size of the vacancy cluster. The fitting curve for the capture radius is obtained as a function of the number of vacancies in the cluster.

Keywords: point defect recombination, bcc iron, reaction radius, kinetic Monte Carlo

(Some figures may appear in colour only in the online journal)

1. Introduction

Radiation-induced property changes occur as a result of the accumulation of point defects under irradiation. The fundamental physical events in irradiated materials are migration, coalescence and recombination of point defects and their clusters, as well as their absorption by sinks. The recombination of a Frenkel pair is one of the simplest events. However, there is no general consensus about the recombination radius at the present time. The detailed atomistic processes of recombination also remain uncertain.

The recombination radius of a Frenkel pair is employed as an input parameter in the object kinetic Monte Carlo (OKMC) and mean field rate theory (RT) methods which are useful in examining radiation damage accumulation in neutron irradiated materials. There are several previous studies which have estimated the recombination radius experimentally [1, 2] and numerically [3, 4]. However, each study has obtained a somewhat different value. As a result, various values from $1.0a_0$ to $3.3a_0$ have been used for the recombination radius r_{re} in the numerical simulations [5–10] based on their own insight, where a_0 is the lattice constant of bcc Fe.

The resistivity measurements for neutron irradiated [1] and electron irradiated bcc Fe [2] result in values for the recombination radius of $1.9a_0$ and $3.3a_0$, respectively, based on estimated values of the Frenkel pair recombination volume of $54\Omega_0$ and $300\Omega_0$, where Ω_0 is the atomic volume. The radius of $3.3a_0$ has been often used both in RT and OKMC [9, 10]. Molecular dynamics (MD) simulation has also been used to estimate the recombination volume, and the corresponding recombination radius becomes $r_{re} = 1.9a_0$ [3]. The comparison of displacement cascade simulation results from binary collision approximation and MD simulations suggests a value of $r_{re} = 3.0$–$3.5a_0$ [4]. In addition, the temperature dependence of the recombination radius has been discussed using the theory of elasticity [11]. Some radius increase is theoretically derived in the low temperature region in copper due to the elastic interaction between a self-interstitial atom (SIA) and a vacancy. The suggestion of temperature dependence of the recombination radius is an interesting result for Frenkel pair recombination. However, the use of elasticity neglects the impact of crystal structure which is thought to strongly influence the recombination process. MD and atomistic KMC (AKMC) are suitable for investigating the atomistic details of the recombination process. Recently, Romashka and Yanilkin employed MD to study the spatial distribution of spontaneous recombination sites for a single SIA around a mono-vacancy in bcc Fe [12].

A mono-vacancy is essentially immobile during the recombination process for tens of ns because the jump frequency of a single SIA is three orders of magnitude higher than that of a mono-vacancy at nuclear power plant operating temperatures. In the case of the Frenkel pair recombination, spontaneous recombination sites (SRS) where an SIA spontaneously recombines with a mono-vacancy are located at different positions around the mono-vacancy. The use frequency of each SRS, as well as the spatial distribution of SRSs, are important factors in estimating the recombination radius because each SRS has a different recombination distance. Therefore a statistically significant number of recombination simulations are needed for a detailed recombination analysis. Although MD is useful for examining atomistic scale phenomena, a parameter study with hundreds of repetitive simulations is difficult in terms of the calculation speed.

We apply SEAKMC to simulate the recombination of a Frenkel pair to evaluate the recombination radius, the recombination paths, the temperature dependence and simulation box size dependence. In section 2, the computational procedures such as the details of the simulation parameters and the initial conditions are explained. In section 3, the simulation results for the recombination radius of a Frenkel pair and the recombination paths are discussed. In section 4, the capture radius of a single SIA by vacancy clusters is discussed, and the relation between the capture radius and the number of vacancies in the cluster is shown. In section 5, the temperature dependence and the effect of simulation box size for the recombination radius are discussed. Finally, the results are summarized in section 6.

2. Computational procedure

SEAKMC is one of the on-the-fly atomistic KMC methods that simulate atomistic processes by determining the saddle point energies for all events that could occur in the system [13, 14]. Like MD, the atomic system in SEAKMC is fully described by an appropriate interatomic potential. SEAKMC evaluates the saddle point energy for possible defect transitions using the dimer method [15, 16] at each time step.

The Active Volume (AV) is an essential concept which accelerates the calculations in SEAKMC by reducing the volume of material that must be evaluated. An AV is defined as a local region around each defect in which the presence of the defect influences the energy of the atoms it contains, e.g. it can be related to the strain field of the defect. More specifically, only the atoms inside an AV are used during the saddle point search; the atoms outside the AV are effectively frozen during the search. However, the atoms outside the AV are not ignored since they can relax and interact during the execution of the KMC step. In this way, atoms are included or excluded from an AV based on the impact of the defect on their energy, and AVs can follow the migration of the defects. Based on previous work [13, 14], the radii of AVs for an SIA and a vacancy are set to $4.2a_0$ and $2.7a_0$ respectively. Since it will be shown that the recombination between a SIA and a vacancy occurs at much closer distance than $4.2a_0$, the AV radii adopted here are also suitable to study the recombination reaction.

The transition energies are determined in each AV using the dimer method that investigates the local curvature of the energy landscape and identifies potential saddle points. Since the transition state energies are determined based on the interatomic potential, there is no need to predetermine the catalog of possible reactions and activation energies as must be done for conventional KMC and RT. The influence of strain fields in the crystal is naturally taken into account in this framework. Because the saddle point searches are limited to the AVs, the calculation cost does not always increase with the simulation box size. Once all event probabilities and migration directions for each defect are determined, an event is selected and the simulation time is advanced using the residence-time algorithm [17] the same way as a conventional KMC.

The interatomic potential developed by Ackland and coworkers [18, 19] was employed in the SEAKMC investigation reported here. This potential describes SIA migration behavior well, although the mono-vacancy has a metastable state at the middle of its transition pathway. However, this artifact does not have a significant impact on the recombination results because much higher interstitial mobility means that the vacancy remains essentially at rest during these simulations of a few hundreds of ps. The lattice constant, a_0, is 2.8553 Å and the simulation box size is $16a_0 \times 16a_0 \times 16a_0$ (8192 atoms) if not otherwise specified. The periodic boundary condition is imposed on the simulation box.

3. Recombination radius of a Frenkel pair

The primary simulation configuration involves placing a mono-vacancy and an SIA, separated by a distance of $5a_0$

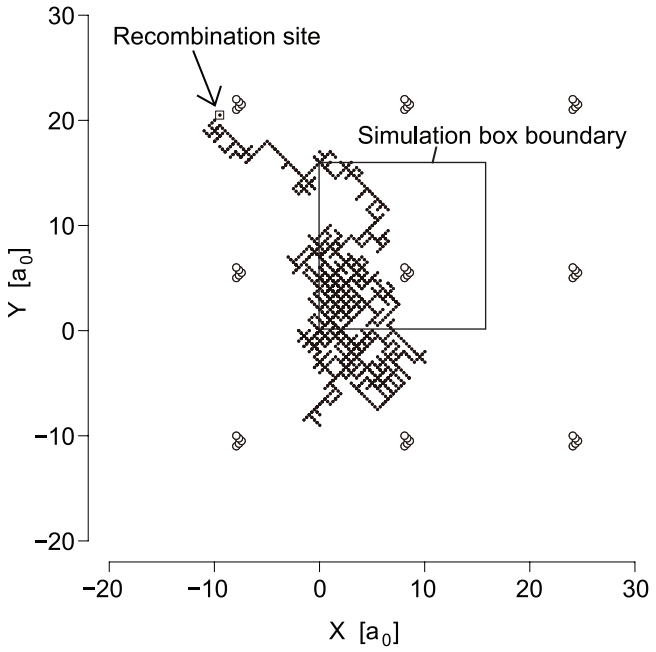

Figure 1. Projection of SIA diffusion trajectory on XY plane. Filled dots show SIA positions and open dots show the vacancy positions. The recombination site of the SIA is indicated by a tiny square mark. Phantom images of the vacancy positions are drawn outside the simulation box to depict the effect of periodic boundary conditions.

in the simulation box of $16a_0 \times 16a_0 \times 16a_0$ at 300 °C. The effect of temperature is introduced only as a variation of T in the transition rate formula, $\nu = \nu_0 \exp(-E_m/k_B T)$, in the same manner as the conventional KMC simulation, where ν is a transition rate, ν_0 is an attempt frequency, E_m is an activation energy and k_B is the Boltzmann factor. Variations in temperature and simulation box size will be discussed below. After initiating the simulation, it continues until they recombine. A total of 80 simulations were performed with each simulation using a different random seed.

Using the current potential in SEAKMC, the migration energy of an isolated SIA is 0.31 eV and that of an isolated vacancy is 0.64 eV. This means that a mono-vacancy jumps only a few times during the recombination simulation up to tens of ns, while an SIA jumps a few hundred times. One of the typical SIA trajectories is shown in figure 1. In this case the SIA approaches the mono-vacancy from the ⟨1 1 1⟩ direction, and they recombined with each other in 28 ns after the simulation started. Let us explain the detailed behavior just before the recombination. After the SIA gets to the tenth nearest neighbor position (abbreviated as 10th-NN hereafter), the SIA dumbbell rotates to another ⟨1 1 0⟩ dumbbell direction on site in the next KMC step. The SIA facing the mono-vacancy results in recombination. The final stable site (FSS) of the SIA was the 10th-NN, and the spontaneous recombination site (SRS) was also the 10th-NN in this case. The FSS is an energetically stable site which an SIA visits just before the recombination, whereas the SRS is an energetically unstable site. It is noted that the SRS is not always located on the same site as the FSS.

Table 1. Case count of SIA trajectories with each FSS and SRS.

FSS (NN)	SRS (NN)	Case count
2nd	2nd	1
4th	2nd	1
4th	4th	9
7th	3rd	1
7th	7th	16
8th	4th	1
8th	7th	2
9th	4th	1
10th	10th	13
11th	7th	3
13th	7th	6
13th	10th	11
17th	10th	14
18th	7th	1

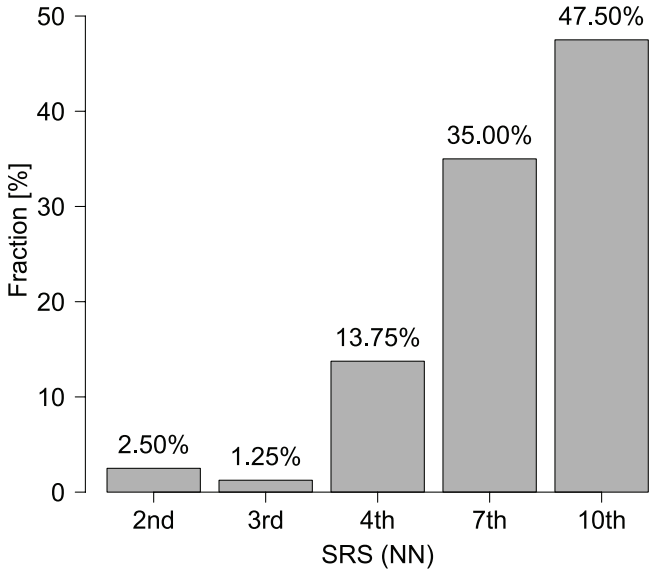

Figure 2. Fraction of each SRS for a Frenkel pair recombination. Values obtained by the summation in terms of SRS in table 1.

The classification in terms of FSS and SRS is useful to understand the recombination process. The results are summarized in table 1. The most frequent path is the way via the 7th-NN (FSS)–7th-NN (SRS), which is 20% of the total cases. In addition, 17th-NN–10th-NN, 10th-NN–10th-NN and 13th-NN–10th-NN are also dominant paths. Categorizing the data in terms of SRS, we found that the SRS is located only at the 2nd-NN, 3rd-NN, 4th-NN, 7th-NN and 10th-NN (figure 2). It is important to note that recombination does not occur every time an SIA arrives at SRS. The direction of the SIA dumbbell must rotate towards the vacancy to recombine. The dominant recombination paths are those in which the SRS is located at the 4th-NN, 7th-NN and 10th-NN; these are illustrated in figure 3. Comparatively long-range recombination occurs from the 10th-NN because the direction toward the vacancy is coincident with the low-energy SIA migration direction of ⟨1 1 1⟩. On the other hand, spontaneous recombination never occurs from the 6th-NN, 8th-NN and 9th-NN

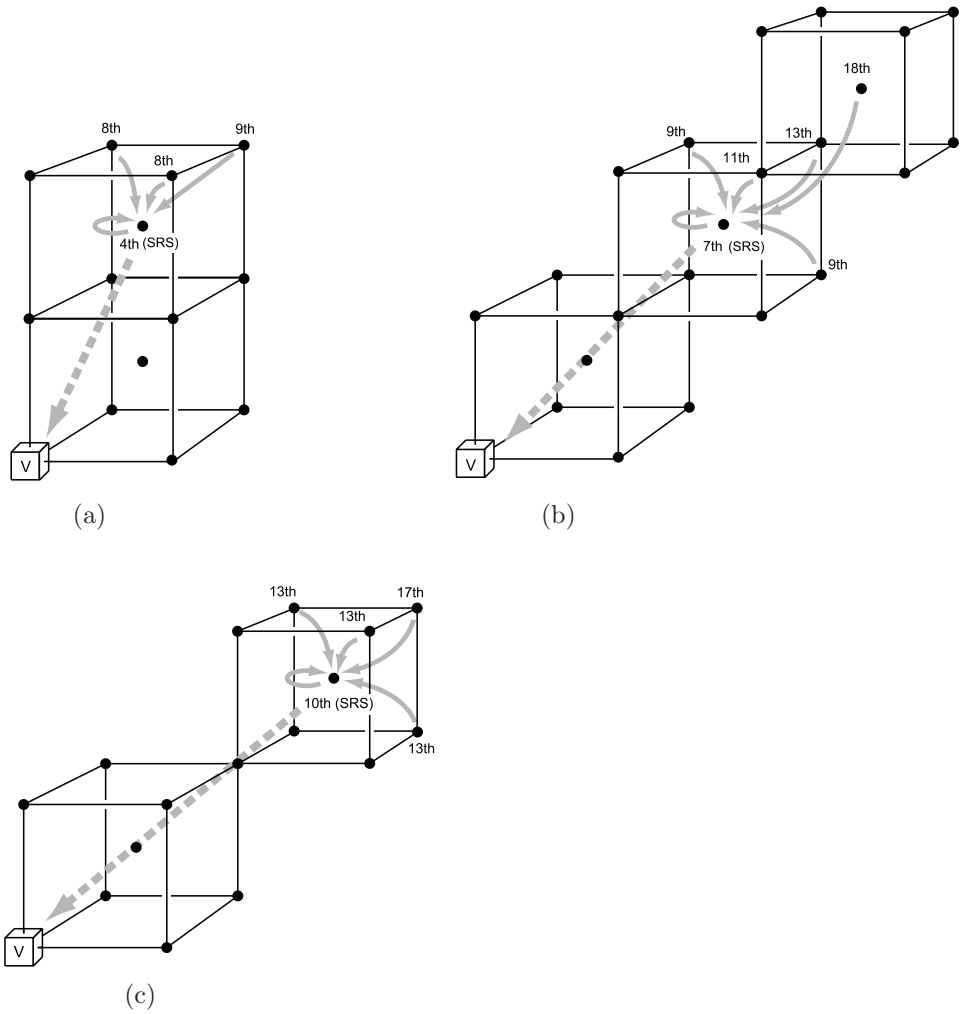

Figure 3. The recombination paths where SRS is located (a) at 4th-NN, (b) at 7th-NN, (c) at 10th-NN. Each small cube with the mark V shows a vacancy site. Labels on the site, *n*th, indicate nearest neighbor orders.

sites. These results suggest that the crystal structure strongly affects the recombination radius.

We define the recombination distance as the distance between the SRS and the mono-vacancy for each simulation case. For instance, the recombination distance is $2.179a_0$ for the case of figure 1 since the SRS was 7th-NN (see appendix A for the correspondence of the nearest neighbor and the distance). Finally the mean recombination radius of a Frenkel pair is determined to be $2.26a_0$ by taking the average of the recombination distance for all 80 cases listed in table 1.

4. Capture radius of an SIA by vacancy clusters

The same sort of analysis used to simulate Frenkel pair recombination was extended to deal with the capture of an SIA by a vacancy cluster. A single SIA is separated by 8 a_0 from a vacancy cluster that consists of 2–5, 10 or 15 vacancies per cluster. The initial configuration of constituent vacancies in each cluster was chosen as the energetically most stable and is pictorially shown in figure 4.

After starting the simulation, the SIA freely migrates in the bcc crystal, until it is captured by the vacancy cluster. The capture radius is defined as a distance between the SRS and the center of mass of the vacancy cluster.

A di-vacancy slightly migrates during the simulation. However, it was never observed to decompose. A tri-vacancy is also mobile, whereas a tetra-vacancy and larger vacancy clusters are immobile.

Taking an average of 16–20 simulation cases with different random seeds for each size, the average value of capture radius for different size vacancy clusters was obtained as listed in table 2. The capture radius gradually increases with the number of vacancies, N, in the cluster.

The capture radius r_c has been proposed in previous studies [7, 9, 10] as a function of N,

$$r_c(N) = \left(\frac{3}{4\pi}\frac{a_0^3}{2}N\right)^{1/3} + \delta. \quad (1)$$

where δ is a constant capture distance from a vacancy cluster surface. The first nearest neighbor $\sqrt{3}a_0/4$ or the lattice constant a_0 is typically used as δ. Although this is a simple arithmetical derivation based on vacancy agglomeration, the assumption of $N^{1/3}$scaling seemed to be reasonable. In addition, we need to consider the effect of strain fields due to

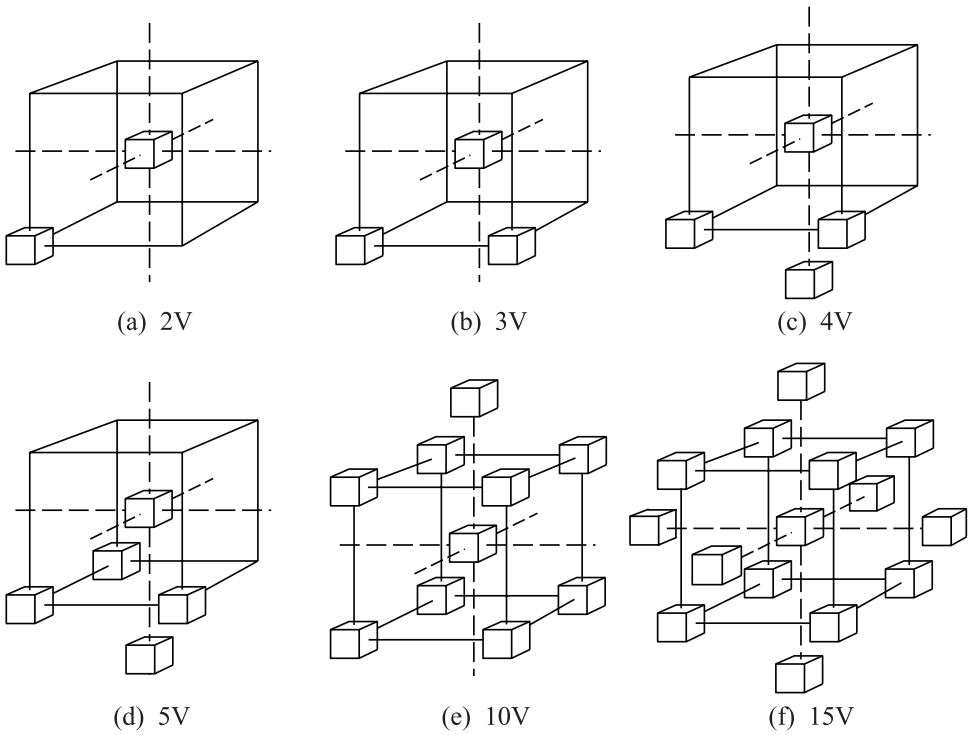

Figure 4. The configuration of vacancies for each cluster size from 2V to 15V. (a) 2V. (b) 3V. (c) 4V. (d) 5V. (e) 10V. (f) 15V.

Table 2. Capture radius and its standard deviations (SD) with N vacancies for each cluster.

N	Capture radius (a_0)	SD
1	2.26	0.41
2	2.39	0.42
3	2.70	0.37
4	2.86	0.36
5	2.85	0.48
10	3.38	0.36
15	3.43	0.37

Note: The capture radius is defined as the distance between SRS and the center of mass of a vacancy cluster.

vacancies and asymmetry of a cluster due to the crystal lattice. These would cause changes to the coefficient of $N^{1/3}$ and δ. Therefore, we propose the following function,

$$r_c'(N) = \alpha N^{1/3} + \delta', \tag{2}$$

where α and δ' are fitting parameters. The values of α and δ' are determined so as to fit the data listed in table 2. By use of nonlinear least squares fitting, we obtained the values of $\alpha = 0.860a_0$ and $\delta' = 1.41a_0$. The fitting curve is plotted in figure 5 together with the conventional curve of equation (1) where we took $\delta = 1.78a_0$ so as to match equations (1) and (2) at $N = 1$ to compare the behavior of the two curves. The curve of equation (1) is found to underestimate the values obtained from our atomistic simulations.

5. Dependence of simulation box size and temperature on recombination radius

The recombination simulations shown in section 3 were carried out with a simulation box of $16a_0 \times 16a_0 \times 16a_0$ at 300 °C. To examine the dependence of the simulation box and the temperature on the recombination radius, five different temperatures of −200 °C, 200 °C, 300 °C, 400 °C and 500 °C, and four simulation box sizes of $10a_0 \times 10a_0 \times 10a_0$, $12a_0 \times 12a_0 \times 12a_0$, $14a_0 \times 14a_0 \times 14a_0$ and $16a_0 \times 16a_0 \times 16a_0$ were prepared. Note that varying the simulation box size is equivalent to varying the defect concentration. We carried out recombination simulations for various combinations of box sizes and temperatures as listed in table 3. Each condition is identified by an ID number in the table.

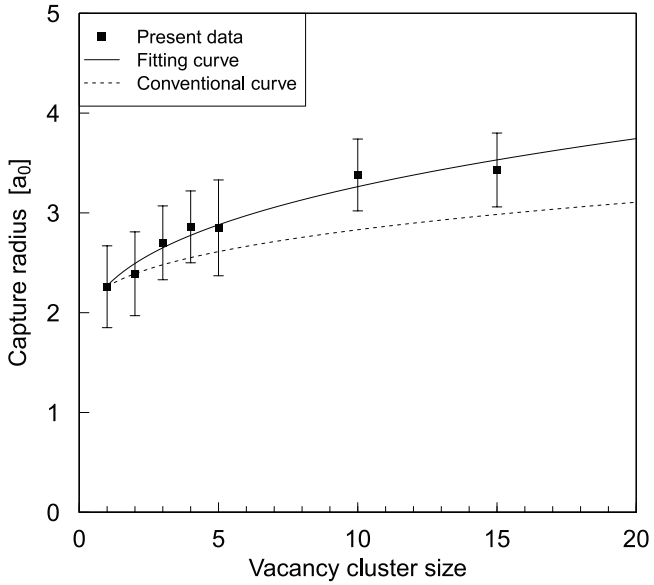

Figure 5. Capture radius of vacancy clusters, the fitting curve (1) and the conventional curve (2). Each error bar shows the standard deviation.

Table 3. The recombination radius obtained for various box sizes and temperatures.

ID	Box size (a_0)	Temperature (°C)	Case count	r_{re} (a_0)	SD (a_0)
1	$10\times10\times10$	200	20	2.13	0.52
2	$10\times10\times10$	300	20	2.31	0.48
3	$10\times10\times10$	400	20	2.26	0.42
4	$10\times10\times10$	500	20	2.18	0.35
5	$12\times12\times12$	200	20	2.15	0.46
6	$12\times12\times12$	300	20	2.24	0.39
7	$12\times12\times12$	400	20	2.16	0.51
8	$12\times12\times12$	500	20	2.33	0.33
9	$14\times14\times14$	200	20	2.23	0.34
10	$14\times14\times14$	300	20	2.28	0.36
11	$14\times14\times14$	400	20	2.36	0.27
12	$14\times14\times14$	500	20	2.15	0.47
13	$16\times16\times16$	200	20	2.05	0.47
14	$16\times16\times16$	300	80	2.26	0.41
15	$16\times16\times16$	400	20	2.21	0.43
16	$16\times16\times16$	500	20	2.20	0.38
17	$16\times16\times16$	−200	20	2.31	0.34
18	$10\times10\times10$	All	80	2.22	0.44
19	$12\times12\times12$	All	80	2.22	0.42
20	$14\times14\times14$	All	80	2.25	0.37
21	$16\times16\times16$	All	140	2.22	0.42
22	All	200	80	2.14	0.45
23	All	300	140	2.27	0.41
24	All	400	80	2.25	0.42
25	All	500	80	2.21	0.39

Note: The ID is a sequence number to identify each condition. The case count is the number of simulations. r_{re} is the recombination radius, and SD is its standard deviation.

The data with ID 1–17 show the recombination radius r_{re} obtained from simulations with the specified box size and temperature. Each recombination radius was taken as an average of 20 simulation cases with the exception of the simulations discussed above with the box size of $16a_0\times16a_0\times16a_0$ at 300 °C, which has 80 cases. In the data with ID 18–21, each recombination radius was obtained from the average of all temperatures with the same box size to confirm the box size dependence. In the data with ID 22–25, each recombination radius was obtained from the average of all box sizes with the same temperature to confirm the temperature dependence.

From this series of parametric studies, neither temperature nor box size dependence was observed on the recombination radius as shown in figure 6. These results suggest that a box size of $16a_0\times16a_0\times16a_0$ is large enough to avoid the periodic boundary effects. We have to qualify our comments about the temperature dependence because the only influence of temperature in these KMC simulations is via the parameter T in the exponential term of the transition rate formula as mentioned in section 3. In reality, as the crystal temperature becomes higher, the lattice parameter increases which may also lead to some variation in ν_0 and E_m. Experimentally, a temperature dependence was observed at less than 100 K in electron irradiated pure Cu [20] although this is a different material. More detailed studies using MD are needed to confirm our observations on the temperature dependence.

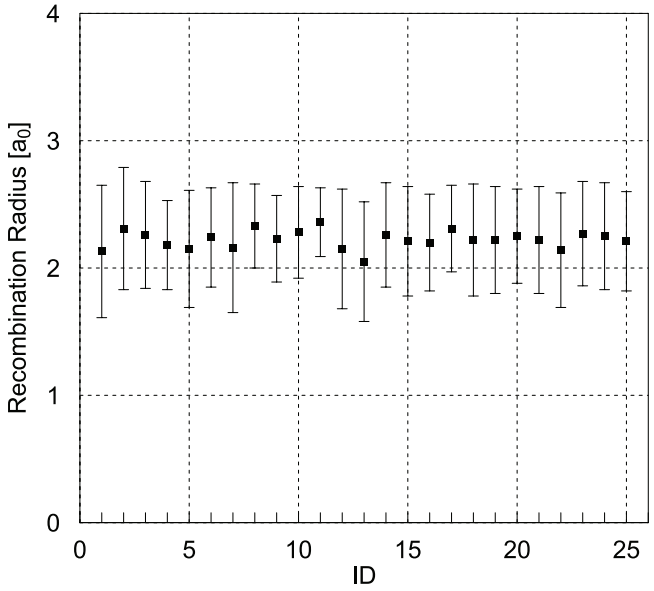

Figure 6. The recombination radius for various box sizes and temperatures. The horizontal axis is assigned according to the ID in table 3.

6. Conclusions

The recombination radius of a Frenkel pair in bcc Fe was determined to be $2.26a_0$ by taking the average of 80 cases of recombination simulations using the SEAKMC method. The spontaneous recombination sites (SRS) are found to be 2nd-NN, 3rd-NN, 4th-NN, 7th-NN and 10th-NN. More than 80% of SIAs are recombined via 7th-NN or 10th-NN positions. These relatively long distances arise because of favorable crystal lattice directions. Romashka and Yanilkin [12] found a smaller recombination volume using a somewhat different procedure in molecular statics simulations because they did not observe spontaneous recombination from sites further than the 7th-NN.

The capture radius of a single SIA by vacancy clusters of different sizes was obtained in the same way as the recombination radius simulations. The capture radius increases with the number of vacancies per cluster N, and its size dependence was found to follow the relationship given in equation (1): $r_c(N) = (0.860N^{1/3} + 1.41)a_0$.

We also examined the dependence of simulation box size (defect concentration) and temperature on Frenkel pair recombination in our simulations. Neither temperature nor box size dependence was observed on the recombination radius in our simulation framework. However, the opportunity for a temperature effect in our KMC simulations is limited. A firm conclusion on the temperature dependence of the recombination radius would require much more lengthy MD simulations.

Finally, it should be mentioned that only a single interatomic potential has been assessed in this work. It is reasonable to expect some sensitivity of the results to the potential chosen since this may influence the details of interstitial migration mechanisms. Additional potentials may be assessed in future work.

Table A1. Distance between the origin and any lattice point d, direction and population of nearest neighbor (NN) sites up to the 20th in bcc crystal.

NN	d (a_0)	Direction	Population
1st	0.866	⟨1 1 1⟩	8
2nd	1.000	⟨1 0 0⟩	6
3rd	1.414	⟨1 1 0⟩	12
4th	1.658	⟨3 1 1⟩	24
5th	1.732	⟨1 1 1⟩	8
6th	2.000	⟨1 0 0⟩	6
7th	2.179	⟨3 3 1⟩	24
8th	2.236	⟨2 1 0⟩	24
9th	2.449	⟨2 1 1⟩	24
10th	2.598	⟨1 1 1⟩	8
10th	2.598	⟨5 1 1⟩	24
11th	2.828	⟨1 1 0⟩	12
12th	2.958	⟨5 3 1⟩	48
13th	3.000	⟨1 0 0⟩	6
13th	3.000	⟨2 1 1⟩	24
14th	3.162	⟨3 1 0⟩	24
15th	3.279	⟨5 3 3⟩	24
16th	3.317	⟨3 1 1⟩	24
17th	3.464	⟨1 1 1⟩	8
18th	3.571	⟨5 5 1⟩	24
18th	3.571	⟨7 1 1⟩	24
19th	3.606	⟨3 2 0⟩	24
20th	3.742	⟨3 2 1⟩	48

Acknowledgments

Research at the Oak Ridge National Laboratory was supported as part of the Center for Defect Physics, an Energy Frontier Research Center funded by the US Department of Energy, Office of Science, Office of Basic Energy Sciences. KN was supported at ORNL by the Central Research Institute of Electric Power Industry.

Appendix A. Location, distance and direction of nearest neighbors in bcc crystal

A direction vector $\boldsymbol{r}$ is given as a vector from an origin which is one of the lattice points to any lattice point around the origin as follows,

$$\boldsymbol{r} = \frac{u}{2}\boldsymbol{a} + \frac{v}{2}\boldsymbol{b} + \frac{w}{2}\boldsymbol{c}, \tag{A.1}$$

where u, v and w are all odd numbers or all even numbers in the case of bcc crystal, and $\boldsymbol{a}$, $\boldsymbol{b}$ and $\boldsymbol{c}$ are orthogonal basis vectors for which the length is equal to the lattice constant, that is, $|\boldsymbol{a}| = |\boldsymbol{b}| = |\boldsymbol{c}| = a_0$.

The distance d is the length of $\boldsymbol{r}$,

$$d = |\boldsymbol{r}| = \sqrt{(u^2 + v^2 + w^2)/4}\,. \tag{A.2}$$

The nearest neighbors (NN) are labeled such as 1st-NN, 2nd-NN and 3rd-NN in ascending order of d. The relationships between NN and their crystallographic parameters, such as Miller indies of lattice point, its population and d are summarized in table A1.

The 10th-NN, 13th-NN and 18th-NN include two different types of sites with the same distance but different directions. These are separately listed.

References

[1] Horak J A and Blewitt T H 1972 *Phys. Status Solidi* a **9** 721
[2] Dural J, Ardonceau J and Jousset J C 1977 *J. Phys. France* **38** 1007
[3] Gao F, Bacon D J, Barashev A V and Heinisch H L 1999 *Mater. Res. Soc. Symp. Proc.* **540** 703
[4] Souidi A, Hou M, Becquart C S and Domain C 2001 *J. Nucl. Mater.* **295** 179
[5] Stoller R E 1993 *Effects of Radiation on Materials: 16th Int. Symp.* (Philadelphia: ASTM) p 394
[6] Soneda N and Díaz de la Rubia T 1998 *Phil. Mag.* A **78** 995
[7] Caturla M J, Soneda N, Alonso E, Wirth B D, Díaz de la Rubia T and Perlado J M 2000 *J. Nucl. Mater.* **276** 13
[8] Hardouin Duparc A, Moingeon C, Smetniansky-de-Grande N and Barbu A 2002 *J. Nucl. Mater.* **302** 143
[9] Domain C, Becquart C S and Malerba L 2004 *J. Nucl. Mater.* **335** 121
[10] Ortiz C J and Caturla M J 2007 *J. Comput.-Aided Mater. Des.* **14** 171
[11] Wolfer W G and Si-Ahmed A 1981 *J. Nucl. Mater.* **99** 117
[12] Romashka M Y and Yanilkin A V 2014 *Phys. Met. Metall.* **115** 965
[13] Xu H, Osetsky Y N and Stoller R E 2011 *Phys. Rev.* B **84** 132103
[14] Xu H, Osetsky Y N and Stoller R E 2012 *J. Phys.: Condens. Matter* **24** 375402
[15] Henkelman G and Jónsson H 1999 *J. Chem. Phys.* **111** 7010
[16] Heyden A, Bell A T and Keil F J 2005 *J. Chem. Phys.* **123** 224101
[17] Bortz A B, Kalos M H and Lebowitz J L 1975 *J. Comput. Phys.* **17** 10
[18] Mendelev M I, Han S, Srolovitz D J, Ackland G J, Sun D Y and Asta M 2003 *Phil. Mag.* **83** 3977
[19] Ackland G J, Mendelev M I, Srolovitz D J, Han S and Barashev A V 2004 *J. Phys.: Condens. Matter* **16** S2629
[20] Lennartz R, Dworschak F and Wollenberger H 1977 *J. Phys. F: Met. Phys.* **7** 2011